Available online at www.sciencedirect.com

SciVerse ScienceDirect

Ceramics International 38 (2012) 5053–5059

CERAMICS INTERNATIONAL

www.elsevier.com/locate/ceramint

Synthesis of hierarchical porous ZnO microspheres and its photocatalytic deNO$_x$ activity

Thi Hang Le [a,1,*], Quang Duc Truong [b,1], Takeshi Kimura [b], Huihui Li [b], Chongsen Guo [b], Shu Yin [b], Tsugio Sato [b], Yong-Chien Ling [a]

[a] *Department of Chemistry, National Tsing Hua University, Hsinchu 30013, Taiwan*

[b] *Institute of Multidisciplinary Research for Advanced Materials, Tohoku University, Sendai 980-8577, Japan*

Received 26 December 2011; received in revised form 2 March 2012; accepted 2 March 2012

Available online 10 March 2012

Abstract

Hierarchical porous metal oxide nanostructures have currently attracted much interest because their unique structures with large surface area, high porosity and low density are greatly valuable for functional applications in catalysis, biological engineering and photoelectronics device. Herein, hierarchical porous ZnO microspheres were fabricated by a facile hydrothermal method with subsequent calcination. The sample morphology has been characterized by scanning electron microscopy and transmission electron microscopy. The powder X-ray diffraction has also been used to determine the crystalline structure of the synthesized materials. The effect of calcination temperature on the crystalline structure of synthesized nanostructures has been systematically investigated. The photocatalytic activities of the obtained samples have been evaluated by means of photocatalytic decomposition of nitrogen monoxide (NO).

Keywords: D. ZnO; Mesoporous; Hierarchical structures; NO decomposition

1. Introduction

Controlling the crystalline structure, size, shape and surface chemistry is currently considered as a central aspect in material science and engineering research. Particularly, morphological control of metal oxides has drawn considerable attentions owing to their versatile ability, stability, efficiency and long-term durability in the wide range of applications [1–4]. Among various ordered structures, hierarchical porous nanostructures are of particular importance due to their unique chemical and physical properties as well as great potential application in catalysis, gas sensing, lithium-ion batteries and photovoltaics devices [1–4]. For example, porous microspheres of TiO_2 have been synthesized with fast, reversible lithium insertion/extraction and enhanced photocatalytic activity [1,2]. The porous iron oxide nanostructures showed an excellent ability to remove various water pollutants [3]. The hierarchical Fe_3O_4/Bi_2O_3 core–shell architectures exhibited powerful visible-light photocatalytic activity for the degradation of rhodamine B [4]. The synthesis of hierarchical porous nanostructures, therefore, has attracted a great attention.

Among various semiconductor metal oxides, zinc oxide is an important semiconductive material with wide band gap, high thermal stability, and excellent catalysis activity [5–9]. Zinc oxide (ZnO) with well-defined nanostructures is one of the most promising candidates for environmental cleanup and energy application [5–9]. To date, various nanostructures of ZnO, such as nanoparticles, nanorods, nanobelts, nanotubes, nanodisks, nanoboxes and hollow sphere structures, have been synthesized [10–14]. However, the well-defined mesoporous structures of ZnO have been rarely reported [15]. It may be due to the fact that ZnO has the strong tendency to grow into one-dimensional nanostructure. Therefore, the synthesis of 3D mesoporous ZnO structures is still considerably difficult. Herein, mesoporous ZnO microspheres were successfully fabricated by a facile hydrothermal method using amino acid as a structure-directing agent with subsequent calcination. Particularly, porous ZnO

* Corresponding author. Tel.: +81 22 217 5597; fax: +81 22 217 5597.
E-mail address: lehang@mail.tagen.tohoku.ac.jp (T.H. Le).

[1] These authors contributed equally to this work.

0272-8842/$36.00
doi:10.1016/j.ceramint.2012.03.007

microspheres have been synthesized by hydrothermal treatment of $Zn(NO_3)_2$ with cysteine followed by a post-synthesis calcination of as-synthesized precipitates. The photocatalytic activity of the obtained ZnO samples has been evaluated by means of decomposition of nitrogen monoxide (NO). The effect of calcination temperature on the crystalline structure and morphology of the synthesized nanostructures was also investigated in detail.

2. Experimental

2.1. Synthetic method

In a typical synthesis, 4 mmol cysteine (99%, Kanto Chemicals Co., Inc.) was dissolved into 25 ml of de-ionized water with continuous stirring. After that, 2 mmol of $Zn(NO_3)_2{\cdot}6H_2O$ (98%, Kanto Chemicals Co., Inc.) was added into as-prepared cysteine solution and the solution was allowed for reaction for 15 min. The obtained transparent solution was placed into a 50 ml Teflon-lined autoclave. The autoclave was heated at 190 °C for 15 h in an electric oven for hydrothermal reaction, then allowed to cool down to room temperature. The precipitates were collected by centrifugation and washed by deionized water/ethanol for several times to remove the excess amount of precursors and residual organic compounds. The obtained particles were finally dried in air at 60 °C for 1 day. For synthesis of ZnO, the obtained precipitates were calcined at 450, 550 and 600 °C for 5 h to remove organic residue and to form ZnO.

2.2. Characterization

The crystalline phase of the samples was characterized using powder X-ray diffraction (XRD; Rigaku RINT V-2200, 40 kV and 30 mA) with Cu Kα radiation (λ = 1.5406 Å). Data were collected in the 2θ–θ scanning mode with a scan speed of 4° min^{-1} and a step size of 0.02°. The morphology of the obtained particles was examined using field-emission scanning electron microscopy (FE-SEM; Hitachi S-4800) at an accelerating voltage of 5 kV. Transmission electron microscopy (TEM; Hitachi H-7650, 100 kV, HR-TEM HF-2000 with selected-area electron diffraction, SAED) was conducted using specimens dispersed in ethanol and then dropped onto Cu microgrids coated with a holey carbon film, followed by evaporation of ethanol. Diffuse reflectance spectra (DRS) of solid samples were evaluated in the range of 200–800 nm with a spectrophotometer instrument Shimadzu, UV 2450. Thermogravimetric analysis (TGA) was measured using DTG-60H (Shimazdu). The sample was heated at a rate of 10 K min^{-1} under N_2 flow of 50 ml min^{-1} up to 1200 °C with Al_2O_3 as a reference. N_2 adsorption and desorption isotherms were measured at 77 K (Micromeritics ASAP 2010) to evaluate the adsorption characteristics, Brunauer–Emmett–Teller (BET) specific surface area and Barrett–Joyner–Halenda (BJH) pore size distribution.

2.3. Decomposition of NO

The synthesized particles were evaluated the photocatalytic activity in terms of oxidative NO decomposition reaction. A glass holder was used to attach samples in a working space (20 mm × 15 mm × 0.5 mm), and set in the center of a sealed plastic reactor of 373 cm^3 volume. A gas current composed of 1 ppm NO in air (balanced N_2) was allowed to flow into the reactor with a flow rate: 200 cm^3 min^{-1}. A 450 W high-pressure mercury lamp was used as a light source. A Pyrex jacket cooled by running water was set around the lamp to cut off UV light (wavelengths $\lambda < 290$ nm). Two removable UV cut-off filters ($\lambda < 400$ nm: 400 nm filter and $\lambda < 510$ nm: 510 nm filter) were placed between the lamp and the reactor if needed. These two removable UV cut-off filters ($\lambda < 400$ nm: 400 nm filter and $\lambda < 510$ nm: 510 nm filter) were employed to cut off the light with undesired wavelength. For example, the light with wavelengths $\lambda < 400$ nm or $\lambda < 510$ nm can be removed using above filters. Therefore, only light with desired wavelengths ($\lambda > 400$ nm or $\lambda > 510$ nm) were irradiated to our reaction system. The remained NO_x concentrations were detected automatically every 10 s using a NO_x analyzer (Yanaco, ECL-88A). After it had been confirmed that the NO_x concentration was constant at approximately 1 ppm in the darkness, the sample was irradiated by visible light using the UV cut-off filters. The NO_x concentration was measured along the irradiation. The 510 and 400 nm filters were respectively removed every 10 min to determine photocatalytic activity of

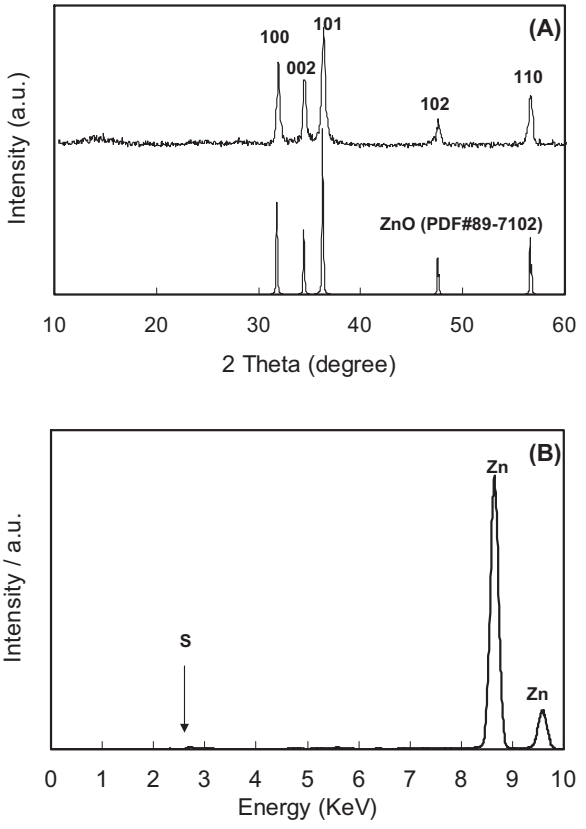

Fig. 1. XRD pattern (A) and EDX pattern (B) of sample prepared by calcination of the precipitates at 550 °C for 5 h.

samples under different irradiated light. The photoreaction finished after 30 min of light irradiation. The experimental setup for NO decomposition has been shown in a previous report [16].

3. Results and discussion

3.1. Characterization of hierarchical ZnO nanostructures

The particles obtained by calcination of as-synthesized precipitates at 550 °C were characterized by powder XRD. Fig. 1A shows the XRD pattern, revealing the presence of the hexagonal structure of ZnO (JCPDS card no. 89-7102) as a single phase. The diffraction peaks can be indexed to {1 0 0}, {0 0 2}, {1 0 1}, {1 0 2} and {1 1 0} of hexagonal structure of ZnO. The EDX pattern of ZnO sample (Fig. 1B) shows the main peak of zinc and very small peak of sulfur indicating that the precipitates have been oxidized to zinc oxide by the calcination.

Fig. 2A and B shows SEM images of the typical hierarchical porous microspheres with different magnifications. The low magnification image (Fig. 2A) reveals that the synthesized particles consist of uniform, interconnected microspheres. The size of microspheres is approximately 5 μm in diameter. The high magnification image (Fig. 2B) implies that such microsphere structures are constructed from nanoparticle building blocks. It can be seen from the surface of the microspheres that the hierarchical structures consist of connected nanoparticles with several tens nanometers in size (Fig. 2B). TEM images (Fig. 2C and D) clearly show the presence of the porous structures, evident from the bright areas in the center of spheres. SAED shown in inset of Fig. 2D reveals the polycrystalline nature of the obtained structures.

The porous ZnO microspheres were further characterized by N_2 gas adsorption analysis, and the results are shown in Fig. 3. The isotherm curve can be categorized as an IUPAC type III with a hysteresis loop in the range of 0.8–1 P/P_0. The BET specific surface area was determined to be 25.9 $m^2\ g^{-1}$. The pore size distribution is narrow with a maximum of about 40–60 nm, which was consistent with microscopy observations.

3.2. Characterization of the obtained precipitates

To investigate the crystalline phase and formula of as-synthesized precipitates, the precipitates obtained by hydrothermal reaction of $Zn(NO_3)_2$ with cysteine at 190 °C were characterized by powder XRD. As shown in Fig. 4A, the diffraction peaks in the XRD pattern of the obtained precipitates are clearly matched to that of the rhombohedral phase of ZnS (JCPDS card no. 89-2427). The EDX pattern (Fig. 4B) of the precipitates indicates that the sample contained

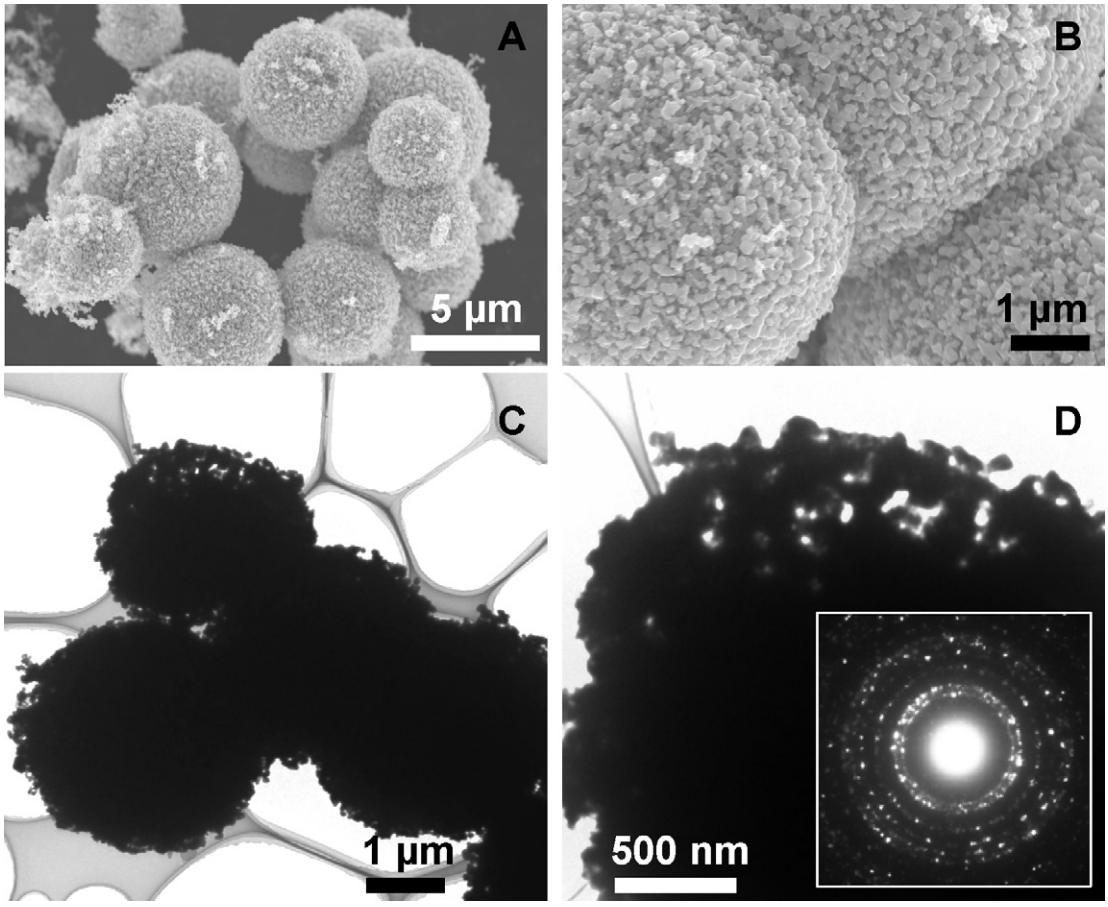

Fig. 2. SEM and TEM images of porous ZnO microspheres prepared by calcination of the precipitates at 550 °C for 5 h. The inset in D shows the selected-area electron diffraction of the corresponding sample.

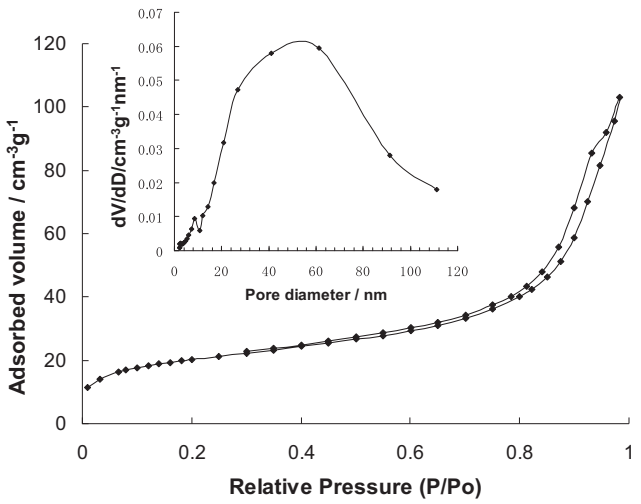

Fig. 3. Adsorption and desorption curves and pore size distribution of porous ZnO microspheres prepared by calcination of the precipitates at 550 °C for 5 h.

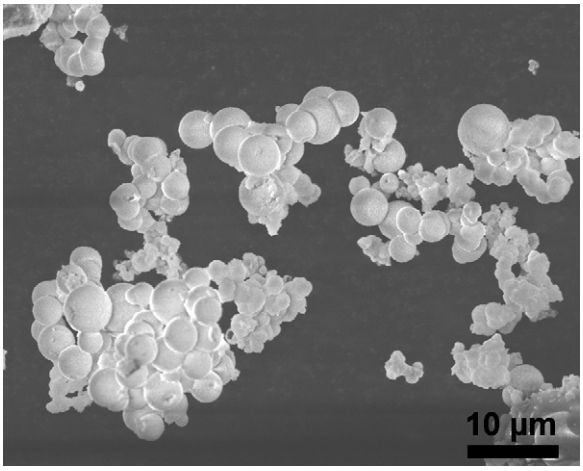

Fig. 5. SEM image of the precipitates obtained by hydrothermal treatment of zinc nitrate and cysteine.

the large amount of zinc and sulfur. Furthermore, the small amount of C was also observed. The precipitates obtained by hydrothermal reaction were also characterized by microscopy as shown in Fig. 5. The as-synthesized particles consist of uniform, interconnected microspheres. The size of microspheres is approximately 5 μm in diameter.

To study the conversion of sulfide to oxide as well as the effect of calcination temperature on the structure of the synthesized particles, TG–DTA analysis has been carried out.

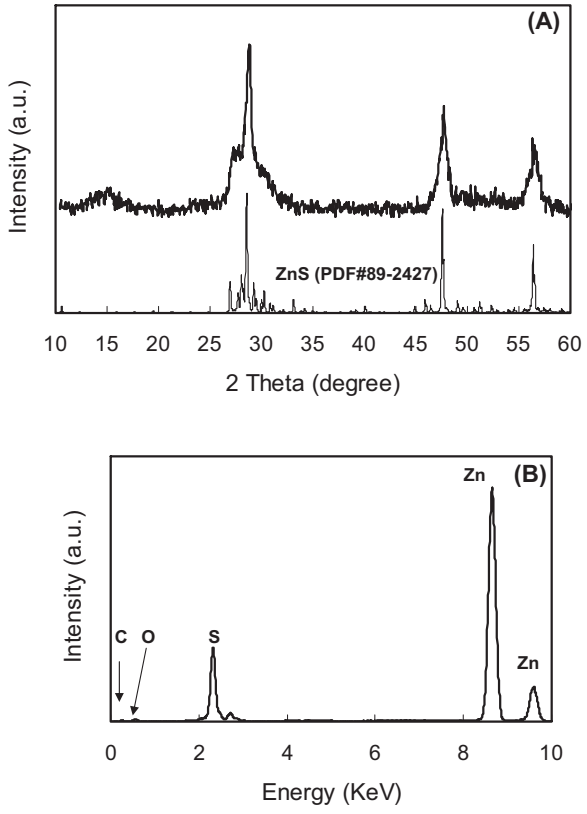

Fig. 4. XRD pattern (A) and EDX pattern (B) of the precipitates obtained by hydrothermal treatment of zinc nitrate and cysteine.

Fig. 6 shows the TG–DTA analysis curves of the sample prepared using $Zn(NO_3)_2$ and cysteine via hydrothermal reaction. TG curve reveals that the sample underwent three stages of the mass-loss process. From room temperature to 200 °C, about 8% of the total mass was lost, which is attributed to the evaporation of the adsorbed water and organic component adsorbed on the surface of particles. The second mass-loss process occurred at 250–450 °C can be assigned to combustion of organic residue on the structures. The third step at 550–650 °C corresponds to the conversion of sulfide to oxide. This process was highly exothermal as revealed in DTA curve.

3.3. The formation of porous ZnO nanostructures

The above analysis supports information to understand the formation mechanism of the present porous structures. As reported recently, biomolecular cysteine-assisted synthesis has been used to prepare various sulfide nanostructures such as Bi_2S_3, PbS and SnS_2 [17–19]. In the present system, cysteine plays dual roles as sulfur source and structure-directing agent. In particular, cysteine has carboxyl (–COOH), hydroxyl (–OH) and thiol group (–SH), which may simultaneously coordinate with Zn^{2+} ions in aqueous solution. For instance, zinc ion has donor–acceptor bond with sulfur atom in thiol group and covalent bond with oxygen atoms of the carboxyl group and/or hydroxyl group in a form of a complex. At the elevated temperature of hydrothermal reaction, the organic component was decomposed, resulting in formation of zinc sulfide (ZnS). ZnS structures were stabilized by organic ligand that adsorbed on the surface of sulfide. The non-covalent bonding such as hydrogen bonding between functional groups is the driving force for the assembly of individual cysteine-coated ZnS nanoparticles into microsphere structures. The ZnS microsphere structures can be easily converted to ZnO structures upon the calcination without the collapse of its 3D hierarchical structures. The removal of organic residue and conversion of ZnS to ZnO by calcination ultimately produces porous structures.

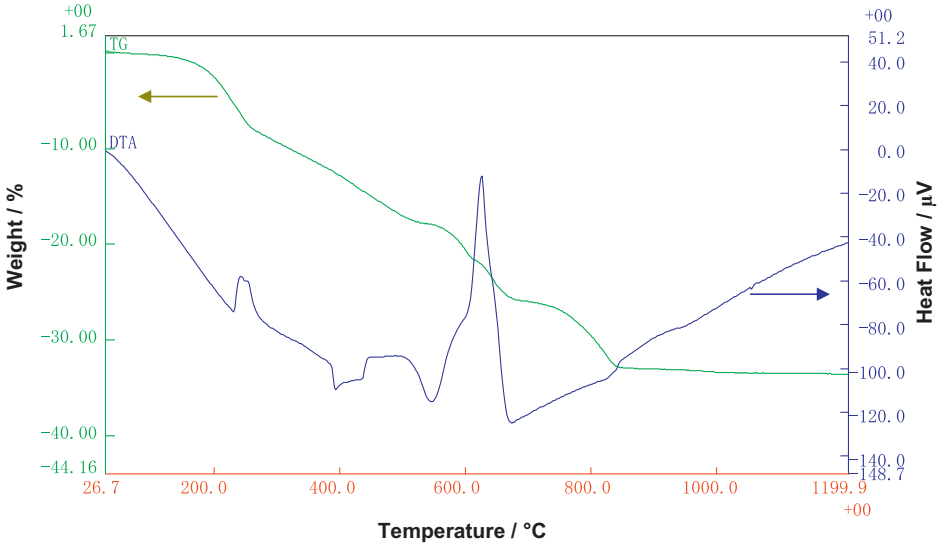

Fig. 6. TG–DTA curves of the precipitates obtained by hydrothermal treatment of zinc nitrate and cysteine.

3.4. Effect of calcinations temperature on the synthesized nanostructures

The calcination temperature plays an important role in determining the crystalline structure as well as morphology of the synthesized particles. For instance, XRD patterns of the particles synthesized at the different temperatures are shown in Fig. 7. XRD pattern of the particles obtained at 450 °C reveals the presence of ZnS rhombohedral structure. This result is consistent with the DTA analysis which shows the conversion of ZnS to ZnO taking place at 550–650 °C. Fig. 8 shows the SEM and TEM images of product that have been synthesized at 450 °C. Only solid ZnS microspheres can be observed. The XRD patterns of particles synthesized at 550 and 600 °C show the appearance of ZnO structures (Fig. 7b and c). It was found that increasing the calcination temperature resulted in the improvement of the crystallinity of the final structures.

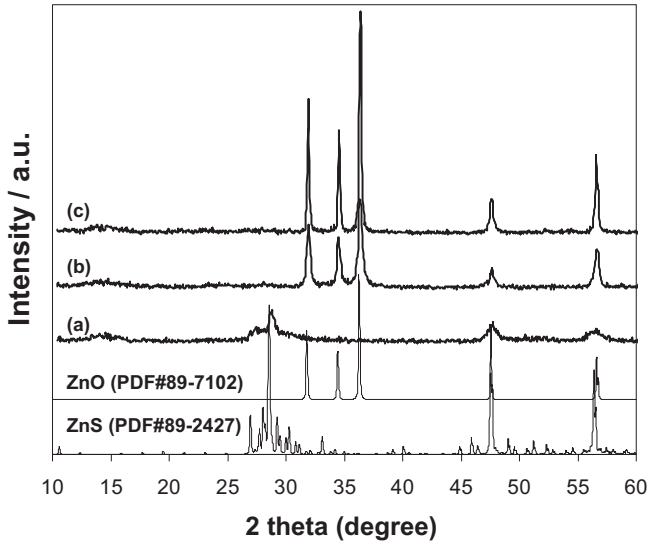

Fig. 7. XRD patterns of the sample prepared by calcination of the precipitates at (a) 450 °C, (b) 550 °C and (c) 600 °C.

3.5. Photocatalytic activity

Diffuse reflectance spectra of the synthesized ZnO in comparison with that of Dugussa P25 are shown in Fig. 9. The P25 (curve a) shows the absorption on UV region only, whereas the synthesized ZnO shows absorption in the entire UV and visible light region. As mentioned above, a small amount of S can be detected in the product obtained at 550 °C (Fig. 1B). Thus, the visible light absorption of ZnO may be attributed to the doping of S in the synthesized structures.

Fig. 10 and Table 1 show the photocatalytic activity of the synthesized particles for the oxidative destruction of NO under irradiation of 450 W high-pressure mercury lamp with visible light of $\lambda > 510$ nm, $\lambda > 400$ nm, and UV light of $\lambda > 290$ nm, respectively. For instance, the residual NO concentration vs. reaction time is displayed in Fig. 10. It can be seen that P25 exhibited high photocatalytic activity under both UV and visible light ($\lambda > 400$ nm) irradiation. The visible light-induced activity of P25 titania might be related to the impurity level caused by the residual impurity such as Cl, which lead formation of Cl-doped TiO_2 [26]. The synthesized ZnO particles had no activity under the irradiation of visible light of $\lambda > 510$ nm. This may be due to the fact that the ZnO is a wide band-gap semiconductor (3.4 eV), i.e., electron–hole pair cannot be generated under visible light irradiation (Fig. 9c). The porous ZnO sample showed the relatively high photocatalytic activity with $deNO_x$ ability of 50.2% and 15.8% under the irradiation of UV–vis and visible light ($\lambda > 400$ nm), respectively. Our group has been studied NO destruction using a variety of photocatalysts, including TiO_2 [16,21–23], $SrTiO_3$ [24–27], etc. Recently, we also performed the photocatalytic $deNO_x$ activity by using LED lamps with precise wavelengths at 627, 530, 445 and 390 nm [26,27]. The photocatalytic decomposition of NO using zinc oxide catalyst has also been

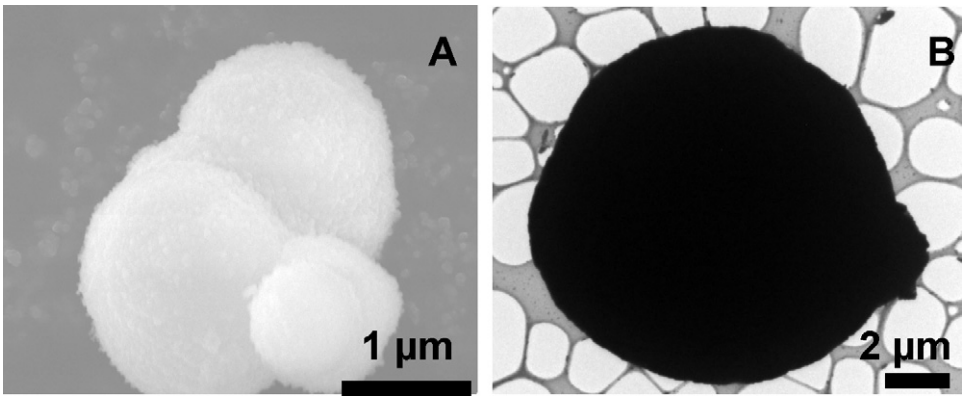

Fig. 8. SEM (A) and TEM (B) images of the sample prepared by calcination of the precipitates at 450 °C.

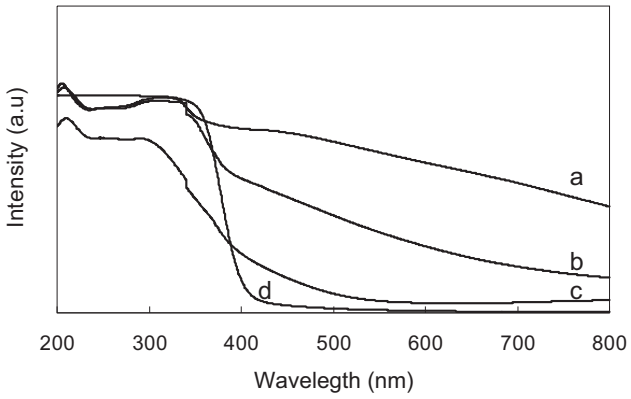

Fig. 9. The UV–vis diffuse reflectance spectra of the precipitates prepared by hydrothermal treatment of zinc nitrate with cysteine (a) and samples obtained by calcination at 450 °C (b); 550 °C (c) and commercial TiO_2-P25 (d).

reported [20]. In a previous study, the photoactivity of various ZnO nanostructures has been investigated [20]. The deNO_x ability on the porous microspheres in the present work is comparable with that of rose-like superstructures. The high photocatalytic activity of the present porous microspheres may be attributed to their unique physical and structural properties with efficient and fast charge transfer ability, resulting from the continuous connecting networks of assembled nanoparticles.

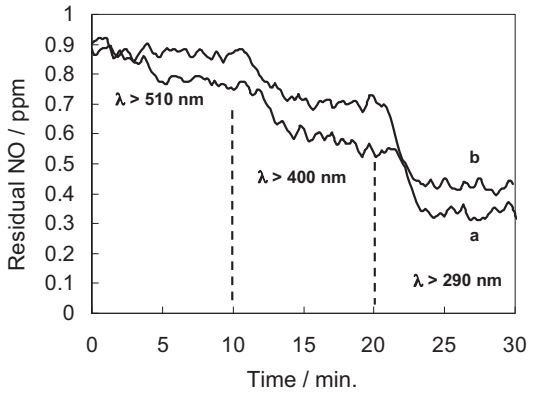

Fig. 10. Photocatalytic NO destruction activity of (a) TiO_2 (Degussa P25) and (b) the porous ZnO microspheres prepared by calcination at 550 °C.

Table 1
Photocatalytic performances and BET specific areas of the catalysts.

Sample	BET ($m^2\ g^{-1}$)	NO destruction ability (%)		
		$\lambda > 290$ nm	$\lambda > 400$ nm	$\lambda > 510$ nm
TiO_2 (P25)	52.6	59.5	35.2	15.0
ZnO	25.9	50.2	15.8	2.1

Thus, electron–hole pair separation was enhanced and driven to react with the adsorbed species, resulting in the enhancement of the photocatalytic activity. Moreover, the presence of hierarchical porous structures can also improve the absorption of light reflections, thus increase light-harvesting ability and final photocatalytic activity. Furthermore, the high surface areas (25.9 $m^2\ g^{-1}$, Table 1) of the obtained particles may also contribute to that remarkable activity because the increase in the number of the catalytic active site on the particles surfaces may allow the efficient transport of photogenerated electrons–holes to the reactant molecules.

The mechanism of photocatalytic deNO_x was mentioned in several reports [22]. Under the irradiation of light, the electron–hole pairs can be generated on the catalyst to form the oxygen radical ($^{\bullet}O_2^-$) and oxohydroxyl radical ($^{\bullet}OOH$). The nitrogen monoxide can react with the reactive oxygen radicals, molecular oxygen, and water in the air to produce HNO_2 and/or HNO_3. It was also reported that about 20% of nitrogen monoxide could be decomposed to nitrogen and oxygen directly [22]. Overall, nitrogen monoxide was photocatalytically converted into non-toxic substances.

4. Conclusion

Synthesis of porous ZnO microspheres with hierarchical nanostructures has been successfully achieved by a facile hydrothermal method followed by thermal treatment. The synthesized hierarchical microspheres with ca. 5 μm in diameters composed of mesoporous structures. Porous ZnO microspheres exhibited a relatively high activity for decomposition of NO under UV–vis light irradiation.

Acknowledgments

Financial support by the National Science Council (NSC 962218E007002 and 974114P007003) of Taiwan is gratefully acknowledged.

References

[1] J.S. Chen, Y.L. Tan, C.M. Li, Y.L. Cheah, D. Luan, S. Madhavi, F.Y.C. Boey, L.A. Archer, X.W. Lou, Constructing hierarchical spheres from large ultrathin anatase TiO_2 nanosheets with nearly 100% exposed (0 0 1) facets for fast reversible lithium storage, J. Am. Chem. Soc. 132 (2010) 6124–6130.

[2] H. Li, Z. Bian, J. Zhu, D. Zhang, G. Li, Y. Huo, H. Li, Y. Lu, Mesoporous titania spheres with tunable chamber structure and enhanced photocatalytic activity, J. Am. Chem. Soc. 129 (2007) 8406–8407.

[3] L.-S. Zhong, J.-S. Hu, H.-P. Liang, A.-M. Cao, W.-G. Song, L.-J. Wan, Self-assembled 3D flowerlike iron oxide nanostructures and their application in water treatment, Adv. Mater. 18 (2006) 2426–2431.

[4] Y. Wang, S. Li, X. Xing, F. Huang, Y. Shen, A. Xie, X. Wang, J. Zhang, Self-assembled 3D flowerlike hierarchical Fe_3O_4@Bi_2O_3 core–shell architectures and their enhanced photocatalytic activity under visible light, Chem. Eur. J. 17 (2011) 4802–4808.

[5] M.H. Huang, S. Mao, H. Feick, H. Yan, Y. Wu, H. Kind, E. Weber, R. Russo, P. Yang, Room-temperature ultraviolet nanowire nanolasers, Science 292 (2001) 1897–1899.

[6] Z.W. Pan, Z.R. Dai, Z.L. Wang, Nanobelts of semiconducting oxides, Science 291 (2001) 1847–1849.

[7] D. Lin, H. Wu, R. Zhang, W. Pan, Enhanced photocatalysis of electrospun Ag–ZnO heterostructured nanofibers, Chem. Mater. 21 (2009) 3479–3484.

[8] P. Sharma, A. Gupta, K.V. Rao, F.J. Owens, R. Sharma, R. Ahuja, J.M. Guillen, B. Johansson, G.A. Gehring, Ferromagnetism above room temperature in bulk and transparent thin films of Mn-doped ZnO, Nat. Mater. 2 (2003) 673–677.

[9] M. Law, L. Greene, J.C. Johnson, R. Saykally, P. Yang, Nanowire dye-sensitized solar cells, Nat. Mater. 4 (2005) 455–459.

[10] W.I. Park, G.C. Yi, Electroluminescence in n-ZnO nanorod arrays vertically grown on p-GaN, Adv. Mater. 16 (2004) 87–90.

[11] M.H. Zhao, Z.L. Wang, S.X. Mao, Piezoelectric characterization of individual zinc oxide nanobelt probed by piezoresponse force microscope, Nano Lett. 4 (2004) 587–590.

[12] G.H. Lee, Synthesis and cathodoluminescence of ZnO tetrapods prepared by a simple oxidation of Zn powder in air atmosphere, Ceram. Int. 37 (2011) 189–193.

[13] J.Q. Hu, Q. Li, X.M. Meng, C.S. Lee, S.T. Lee, Thermal reduction route to the fabrication of coaxial Zn/ZnO nanocables and ZnO nanotubes, Chem. Mater. 15 (2003) 305–308.

[14] J.Q. Hu, Y. Bando, J.H. Zhan, Y.B. Li, T. Sekiguchi, Two-dimensional micrometer-sized single-crystalline ZnO thin nanosheets, Appl. Phys. Lett. 83 (2003) 4414.

[15] Y. Liu, D. Wang, Q. Peng, D. Chu, X. Liu, Y. Li, Directly assembling ligand-free ZnO nanocrystals into three-dimensional mesoporous structures by oriented attachment, Inorg. Chem. 50 (2011) 5841–5847.

[16] S. Yin, H. Hasegawa, D. Maeda, M. Ishitsuka, T. Sato, Synthesis of visible-light-active nanosize rutile titania photocatalyst by low temperature dissolution–reprecipitation process, J. Photochem. Photobiol. A: Chem. 163 (2004) 1–8.

[17] B. Zhang, X.C. Ye, W.Y. Hou, Y. Zhao, Y. Xie, Biomolecule-assisted synthesis and electrochemical hydrogen storage of Bi_2S_3 flowerlike patterns with well-aligned nanorods, J. Phys. Chem. B 110 (2006) 8978–8985.

[18] F. Zuo, S. Yan, B. Zhang, Y. Zhao, Y. Xie, L-Cysteine-assisted synthesis of PbS nanocube-based pagoda-like hierarchical architectures, J. Phys. Chem. C 112 (2008) 2831–2835.

[19] Y.Q. Lei, S.Y. Song, W.Q. Fan, Y. Xing, H.J. Zhang, Facile synthesis and assemblies of flowerlike SnS_2 and In^{3+}-doped SnS_2, J. Phys. Chem. C 113 (2009) 1280–1285.

[20] T. Long, X. Dong, X. Liu, J. Liu, S. Yin, T. Sato, Synthesis of ZnO crystals with unique morphologies by a low-temperature solvothermal process and their photocatalytic deNO_x properties, Res. Chem. Intermed. 36 (2010) 61–67.

[21] Y. Aita, M. Komatsu, S. Yin, T. Sato, Phase-compositional control and visible light photocatalytic activity of nitrogen-doped titania via solvothermal process, J. Solid State Chem. 177 (2004) 3235–3238.

[22] S. Yin, Y. Aita, M. Komatsu, J. Wang, Q. Tang, T. Sato, Synthesis of excellent visible-light responsive $TiO_{2-x}N_y$ photocatalyst by a homogeneous precipitation–solvothermal process, J. Mater. Chem. 15 (2005) 674–682.

[23] H.H. Li, S. Yin, T. Sato, Novel luminescent photocatalytic deNO_x activity of $CaAl_2O_4$:(Eu, Nd)/$TiO_{2-x}N_y$ composite, Appl. Catal. B: Environ. 106 (2011) 586–591.

[24] J. Wang, S. Yin, Q. Zhang, F. Saito, T. Sato, Mechanochemical synthesis of $SrTiO_{3-x}F_x$ with high visible light photocatalytic activities for nitrogen monoxide destruction, J. Mater. Chem. 13 (2003) 2348–2352.

[25] J. Wang, S. Yin, M. Komatsu, Q. Zhang, F. Saito, T. Sato, Photo-oxidation properties of nitrogen doped $SrTiO_3$ made by mechanical activation, Appl. Catal. B: Environ. 52 (2004) 11–21.

[26] U. Sulaeman, S. Yin, T. Sato, Solvothermal synthesis of designed non-stoichiometric strontium titanate for efficient visible-light photocatalysis, Appl. Phys. Lett. 97 (2010) 103102.

[27] U. Sulaeman, S. Yin, T. Sato, Visible light photocatalytic activity induced by the carboxyl group chemically bonded on the surface of $SrTiO_3$, Appl. Catal. B: Environ. 102 (2011) 286–290.